

# Gravitational Waves from Hidden QCD Phase Transition

Mayumi Aoki,<sup>\*</sup> Hiromitsu Goto,<sup>†</sup> and Jisuke Kubo<sup>‡</sup>

*Institute for Theoretical Physics, Kanazawa University, Kanazawa 920-1192, Japan*

## Abstract

Drastic changes in the early universe such as first-order phase transition can produce a stochastic gravitational wave (GW) background. We investigate the testability of a scale invariant extension of the standard model (SM) using the GW background produced by the chiral phase transition in a strongly interacting QCD-like hidden sector, which, via a SM singlet real scalar mediator, triggers the electroweak phase transition. Using the Nambu–Jona-Lasinio method in a mean field approximation we estimate the GW signal and find that it can be tested by future space based detectors.

arXiv:1709.07572v1 [hep-ph] 22 Sep 2017

---

<sup>\*</sup>Electronic address: mayumi@hep.s.kanazawa-u.ac.jp

<sup>†</sup>Electronic address: goto@hep.s.kanazawa-u.ac.jp

<sup>‡</sup>Electronic address: jik@hep.s.kanazawa-u.ac.jp

## I. INTRODUCTION

It is a challenge for physics beyond the standard model (SM) to answer a long-standing question — what is the origin of mass? The same question applies to dark matter (DM), which, if it is particle, is absent in the SM. Though various suggestions how to go beyond the SM exist, there is so far no sign for that from the Large Hadron Collider (LHC) experiments [1, 2] and no sign from the current DM detection experiments either [3, 4].

In contrast to this situation, the first observation of the gravitational wave (GW) signal at LIGO [5] has opened a new way to study astrophysical phenomena and has awaked the hope in particle cosmology that phenomena in the early universe can also be probed by the GW. It has been indeed known that phenomena in the early universe such as inflation [6], topological defects [7] and first-order phase transition [8] generate a non-localized stochastic GW background. Especially, phase transitions in particle physics are associated with symmetry breaking, and therefore the GW signals produced by these phase transitions can be an alternative approach to investigate the structure of symmetries in the early universe. Unfortunately, because of not being first order, the phase transition associated with the electroweak (EW) symmetry breaking in the SM can not produce the GW background [9–11]. However, if the SM is extended, observable GW signals associated with the EW symmetry breaking may be produced and tested in future experiments such as LISA [12, 13] and DECIGO [14–16] as discussed in [17–29].

As lattice simulations in QCD have shown [30–32], the chiral phase transition in QCD is, due to a relatively large current mass of the strange quark, cross over type. This does not prevent the possibility that the chiral phase transition in a QCD-like hidden sector is of first order. In fact, such a possibility with a critical temperature of  $\mathcal{O}(1)$  TeV has been recently found [33, 34] in a scale invariant extension of the SM [33–39], in which dynamical chiral symmetry breaking ( $D\chi$ SB) in a QCD-like hidden sector triggers the EW symmetry breaking. In the present paper we focus on this model. In this model, moreover, the EW energy scale and the DM mass have the same origin. In the most of the parameter space the DM mass is created before the EW phase transition and, in a certain region of the parameter space, it takes place during a strong first-order chiral phase transition. By choosing various benchmark points in the parameter space we study the testability of the GW background produced by this phase transition.

The paper is organized as follows. In Sec. II we briefly review the scale invariant extension of the SM with a QCD-like hidden sector and how we use the Nambu–Jona-Lasinio (NJL) model [40–42] as an effective low-energy theory in a mean field approximation [43, 44]. We fix the number of the hidden color  $n_c$  and flavor  $n_f$  both at three, because we can simply rescale the values of the NJL parameters for the real hadrons. In this way we can avoid increasing the number of the independent parameters when going from the high-energy theory to the low-energy effective theory. We pick up a set of four benchmark parameters, for which the chiral phase transition in the hidden QCD sector is of first order. For these points we calculate the GW signals.

Note that the chiral phase transition in our model occurs in a two-dimensional parameter space, the chiral condensate and the vacuum expectation value (VEV) of the SM singlet real scalar (which is the mediator of the energy scale from the hidden sector to the SM sector). Furthermore, the mean field  $\sigma$  corresponding to the chiral condensate is a non-propagating field at the zero-th order in the mean field approximation: It becomes a quantum field at the one-loop level, so that its wave function renormalization constant is far from one and depends on the mean fields as well as on the temperature. In Sec. III we discuss how to manage the complications mentioned above to compute the rate of the bubble nucleation that occurs during the cosmological tunneling in the hidden QCD sector. In Sec. IV we discuss the detectability of the GW signals produced by the chiral phase transition for the benchmark points in the parameter space. We summarize and conclude in Sec. V.

## II. THE MODEL

We consider a classically scale invariant extension of the SM studied in [33–37], which consists of a hidden  $SU(n_c)_H$  gauge sector coupled via a real singlet scalar field  $S$  to the SM. The Lagrangian of the hidden sector is written as

$$\mathcal{L}_H = -\frac{1}{2}\text{Tr } F^2 + \text{Tr } \bar{\psi} (i\not{D} - yS) \psi, \quad (1)$$

where the hidden vector-like fermions  $\psi_i$  ( $i = 1, \dots, n_f$ ) transform as a fundamental representation of  $SU(n_c)_H$ . The  $\mathcal{L}_{\text{SM}+S}$  part of the total Lagrangian  $\mathcal{L}_T = \mathcal{L}_{\text{SM}+S} + \mathcal{L}_H$  contains the SM gauge and Yukawa interactions along with the scalar potential

$$V_{\text{SM}+S} = \lambda_H (H^\dagger H)^2 + \frac{1}{4} \lambda_S S^4 - \frac{1}{2} \lambda_{HS} S^2 (H^\dagger H), \quad (2)$$

where  $H^T = (H^+, (h + G)/\sqrt{2})$  is the SM Higgs doublet field with  $H^+$  and  $G$  as the would-be Nambu-Goldstone (NG) fields. The scalar couplings at the tree-level have to satisfy the stability condition for the scalar potential

$$\lambda_H > 0, \quad \lambda_S > 0 \quad \text{and} \quad 2\sqrt{\lambda_H \lambda_S} - \lambda_{HS} > 0. \quad (3)$$

Here  $y$  and  $\lambda_{HS}$  are assumed to be positive. This model explains the origin of the mass of the Higgs boson and the DM in the following sense.

- First, due to the  $D\chi SB$  in the hidden sector, a non-zero chiral condensate  $\langle \bar{\psi}\psi \rangle$  forms and generates a mass scale above the EW scale. Consequently, NG bosons, which are mesons in the hidden sector, appear.
- At the same time of the hidden  $D\chi SB$ , the singlet scalar field  $S$  acquires a non-zero VEV  $\langle S \rangle$  because of the Yukawa interaction  $-yS\bar{\psi}\psi$ . Note that the Yukawa interaction breaks the chiral symmetry explicitly, and  $y\langle S \rangle$  plays a role of a current mass. Therefore, the mass of the hidden mesons depends crucially on  $y\langle S \rangle$ .
- These hidden mesons (or a part of them) can become DM candidates, because they are stable due to the vector-like flavor symmetry that is left unbroken after the  $D\chi SB$ .
- The EW symmetry breaking is triggered by the Higgs mass term that is nothing but the scalar coupling  $+\frac{1}{2}\lambda_{HS}S^2H^\dagger H$  with the non-zero  $\langle S \rangle$ .

In this work we consider the case with  $n_c = n_f = 3$  and assume that the singlet scalar  $S$  equally couples to the hidden fermions. Then the hidden chiral symmetry  $SU(3)_L \times SU(3)_R$  is dynamically broken down to  $SU(3)_V$ , and thanks to this unbroken symmetry, eight hidden pions become a DM candidate. The DM physics and the impact of the hidden chiral phase transition to the EW phase transition have been investigated in [33] by using the NJL theory [40–42] in the self-consistent mean field (SCMF) approximation [43, 44]. It has been found that a strong first-order chiral phase transition can occur if the Yukawa coupling  $y$  is small enough, i.e.,  $y \lesssim 0.006$  [34]. Within the framework of the NJL theory we will calculate the GW spectrum produced by the hidden chiral phase transition later on. The same model has been analyzed by using a linear [35] and non-linear [36] sigma model and also AdS/QCD approach [39]. In [45], the GW spectrum from the hidden chiral phase transition has been calculated within the framework of a linear sigma model.

### A. Nambu–Jona-Lasinio Lagrangian in a mean field approximation

Following [33] we approximate the high energy Lagrangian (1) by the NJL Lagrangian

$$\mathcal{L}_{\text{NJL}} = \text{Tr } \bar{\psi} (i\cancel{\partial} - yS) \psi + 2G \text{Tr } \Phi^\dagger \Phi + G_D (\det \Phi + h.c.), \quad (4)$$

where  $G$  and  $G_D$  are dimensional parameters and

$$\begin{aligned} (\Phi)_{ij} &= \bar{\psi}_i (1 - \gamma_5) \psi_j = \frac{1}{2} \lambda_{ji}^a \text{Tr } \bar{\psi} \lambda^a (1 - \gamma_5) \psi, \\ (\Phi^\dagger)_{ij} &= \bar{\psi}_i (1 + \gamma_5) \psi_j = \frac{1}{2} \lambda_{ji}^a \text{Tr } \bar{\psi} \lambda^a (1 + \gamma_5) \psi. \end{aligned}$$

Here  $\lambda^a$  ( $a = 1, \dots, 8$ ) are the Gell-Mann matrices with  $\lambda^0 = \sqrt{2/3}$ . To deal with the NJL Lagrangian (4), which is non-renormalizable, we work in the SCMF approximation [43, 44]. The mean fields  $\sigma$  and  $\phi_a$  are defined in the “BCS” vacuum as

$$\langle \Phi \rangle = -\frac{1}{4G} \left( \text{diag}(\sigma, \sigma, \sigma) + i (\lambda^a)^T \phi_a \right). \quad (5)$$

After splitting up the NJL Lagrangian into the sum  $\mathcal{L}_{\text{NJL}} = \mathcal{L}_{\text{MFA}} + \mathcal{L}_I$ , where  $\mathcal{L}_{\text{MFA}}$  contains at most bilinear terms of  $\psi_i$  and  $\mathcal{L}_I$  is normal ordered with respect to the BCS vacuum, we find the Lagrangian in the SCMF approximation:

$$\begin{aligned} \mathcal{L}_{\text{MFA}} &= \text{Tr } \bar{\psi} (i\cancel{\partial} - M) \psi - i \text{Tr } \bar{\psi} \gamma_5 \phi \psi - \frac{1}{8G} \left( 3\sigma^2 + 2 \sum_{a=1}^8 \phi_a \phi_a \right) \\ &\quad + \frac{G_D}{8G^2} \left( -\text{Tr } \bar{\psi} \phi^2 \psi + \sum_{a=1}^8 \phi_a \phi_a \text{Tr } \bar{\psi} \psi + i\sigma \text{Tr } \bar{\psi} \gamma_5 \phi \psi + \frac{\sigma^3}{2G} + \frac{\sigma}{2G} \sum_{a=1}^8 (\phi_a)^2 \right), \end{aligned} \quad (6)$$

where  $\phi = \sum_{a=1}^8 \phi_a \lambda^a$ , we have suppressed  $\phi_0$  here, and  $M$  is given by

$$M = \sigma + yS - \frac{G_D}{8G^2} \sigma^2. \quad (7)$$

Through integrating out the hidden fermions, a non-trivial correction to the tree-level potential for  $\sigma$  is generated, such that the position of the potential minimum can be shifted from zero to a finite value of  $\sigma$ . From the definition (5) we see that this is nothing but the chiral condensate in the SCMF approximation. By self-consistency it is meant that the actual value of  $\langle \sigma \rangle$  is computed afterwards at the loop-level, and then we consider the mean field Lagrangian (6) around this mean field vacuum. At the tree level of (6), the mean fields  $\sigma$  and  $\phi_a$  are non-propagating classical fields. Through integrating out the hidden fermions at the one-loop level, their kinetic terms are also generated. At this stage we reinterpret them as propagating quantum fields.

## B. Mass Spectrum

The chiral condensation in the hidden sector can be studied by using the one-loop effective potential obtained from the mean field Lagrangian (6):

$$V_{\text{eff}} = V_{\text{SM}+S} + V_{\text{NJL}}, \quad (8)$$

where

$$V_{\text{NJL}}(\sigma, S; \Lambda_{\text{H}}) = \frac{3}{8G}\sigma^2 - \frac{G_D}{16G^3}\sigma^3 - 3n_c I_0(M; \Lambda_{\text{H}}), \quad (9)$$

and  $I_0$  is given by

$$I_0(M; \Lambda) = \frac{1}{16\pi^2} \left[ \Lambda^4 \ln \left( 1 + \frac{M^2}{\Lambda^2} \right) - M^4 \ln \left( 1 + \frac{\Lambda^2}{M^2} \right) + \Lambda^2 M^2 \right]. \quad (10)$$

Here we have used the four-dimensional cutoff, and  $\Lambda$  is the corresponding cutoff parameter. The NJL parameters for the hidden QCD is obtained by scaling-up the values of  $G, G_D$  and  $\Lambda$  for the real hadrons. That is, we assume that the dimensionless combinations

$$G^{1/2}\Lambda = 1.82, \quad (-G_D)^{1/5}\Lambda = 2.29, \quad (11)$$

which are satisfied for the real hadrons, remain unchanged for a higher scale of  $\Lambda$ . For a given set of the free parameters of the model  $\lambda_H, \lambda_{HS}, \lambda_S$  and  $y$ , the VEV of  $\sigma$  and  $S$  can be determined through the minimization of the scalar potential  $V_{\text{eff}}(h, S, \sigma; \Lambda_{\text{H}})$ , where the hidden QCD scale  $\Lambda_{\text{H}}$  is so chosen to satisfy  $\langle h \rangle = 246$  GeV.

The mass spectrum of the particles can be computed from the corresponding two point functions, which are obtained by integrating out the hidden fermions. Note that the CP even scalars  $h, S$  and  $\sigma$  mix with each other. The flavor eigenstates  $\varphi_i$  ( $i = h, S, \sigma$ ) and the mass eigenstates  $s_i$  ( $i = 1, 2, 3$ ) are related by  $\varphi_i = \xi_i^{(j)} s_j$ . Their masses are determined by the zeros of the two point functions  $\Gamma_{ij}$  ( $i, j = h, S, \sigma$ ) at the one-loop level, i.e.  $\Gamma_{ij}(m_k^2) \xi_j^{(k)} = 0$ , where

$$\begin{aligned} \Gamma_{hh}(p^2) &= p^2 - 3\lambda_H \langle h \rangle^2 + \frac{1}{2}\lambda_{HS} \langle S \rangle^2, \quad \Gamma_{hS} = \lambda_{HS} \langle h \rangle \langle S \rangle, \quad \Gamma_{h\sigma} = 0, \\ \Gamma_{SS}(p^2) &= p^2 - 3\lambda_S \langle S \rangle^2 + \frac{1}{2}\lambda_{HS} \langle h \rangle^2 - y^2 3n_c I_{\varphi^2}(p^2, M; \Lambda_{\text{H}}), \\ \Gamma_{S\sigma}(p^2) &= -y \left( 1 - \frac{G_D \langle \sigma \rangle}{4G^2} \right) 3n_c I_{\varphi^2}(p^2, M; \Lambda_{\text{H}}), \\ \Gamma_{\sigma\sigma}(p^2) &= -\frac{3}{4G} + \frac{3G_D \langle \sigma \rangle}{8G^3} - \left( 1 - \frac{G_D \langle \sigma \rangle}{4G^2} \right)^2 3n_c I_{\varphi^2}(p^2, M; \Lambda_{\text{H}}) \\ &\quad + \frac{G_D}{G^2} 3n_c I_V(M; \Lambda_{\text{H}}), \end{aligned} \quad (12)$$

and the loop functions are defined as

$$I_{\varphi^2}(p^2, M; \Lambda) = \int_{\Lambda} \frac{d^4 k}{i(2\pi)^4} \frac{\text{Tr}(\not{k} + \not{p} + M)(\not{k} + M)}{((k+p)^2 - M^2)(k^2 - M^2)}, \quad (13)$$

$$I_V(M; \Lambda) = \int_{\Lambda} \frac{d^4 k}{i(2\pi)^4} \frac{M}{(k^2 - M^2)} = -\frac{1}{16\pi^2} M \left[ \Lambda^2 - M^2 \ln \left( 1 + \frac{\Lambda^2}{M^2} \right) \right]. \quad (14)$$

We identify the SM Higgs with the mass eigenstate corresponding to  $\xi_1$  which is supposed to be most close to  $(1, 0, 0)$ , and its mass is  $m_1 = m_h = 125.09 \pm 0.24$  GeV [46]. Similarly we use:  $m_2 = m_S$  and  $m_3 = m_{\sigma}$ . The DM candidate is the hidden pion  $\phi_a$  and its mass is also generated at the one-loop level. Its two point function is

$$\Gamma_{\text{DM}}(p^2) = -\frac{1}{2G} + \frac{G_D \langle \sigma \rangle}{8G^3} + \left( 1 - \frac{G_D \langle \sigma \rangle}{8G^2} \right)^2 2n_c I_{\phi^2}(p^2, M; \Lambda_H) + \frac{G_D}{G^2} n_c I_V(M; \Lambda_H), \quad (15)$$

where the loop function is given by

$$I_{\phi^2}(p^2, M; \Lambda) = \int_{\Lambda} \frac{d^4 k}{i(2\pi)^4} \frac{\text{Tr}(\not{k} - \not{p} + M)\gamma_5(\not{k} + M)\gamma_5}{((k-p)^2 - M^2)(k^2 - M^2)}. \quad (16)$$

Then we can calculate the DM mass from  $\Gamma_{\text{DM}}(m_{\text{DM}}^2) = 0$ .

Once the set of the parameters  $(\lambda_H, \lambda_{HS}, \lambda_S, y)$  is given, the mass spectrum of the hidden sector particles is fixed. Figure 1 shows the Yukawa coupling  $y$  dependence of the DM mass  $m_{\text{DM}}$  and the mediator mass  $m_S$  (left) and the hidden QCD scale  $\Lambda_H$  (right) for  $\lambda_H = 0.13$ ,  $\lambda_S = 0.08$  and  $\lambda_{HS} = 0.001$  (solid lines), 0.002 (dashed lines). As shown in Fig. 1 (left), the DM mass  $m_{\text{DM}}$  is proportional to the Yukawa coupling  $y$ . This is because the Yukawa interaction breaks the chiral symmetry explicitly. The scale of the D $\chi$ SB in the hidden sector, which is the hidden QCD scale  $\Lambda_H$ , depends on how the mediator  $S$  transfers the mass scale to the SM sector. The larger couplings  $\lambda_{HS}$  and  $y$  are, the closer to the EW scale the hidden QCD scale  $\Lambda_H$  locates as seen in Fig. 1 (right). Moreover the annihilation processes of the DM also depend on the mass spectrum and the Yukawa coupling  $y$ . Note that the one-loop effective couplings are given by  $\Gamma_{\phi\phi S} \propto y$  and  $\Gamma_{\phi\phi SS} \propto y^2$ . In the small  $y$  area with  $m_S > m_{\text{DM}}$ , the mass spectrum should satisfy the resonance condition  $m_S \simeq 2m_{\text{DM}}$  to obtain a realistic DM relic abundance and, in this parameter space, the spin-independent cross section of DM off the nucleon becomes so small [33] that it will be very difficult to detect DM at direct DM detection experiments such as XENON1T [4]. On the other hand, the GW signal might be observed since a strong first-order chiral phase transition can appear for small  $y$  area [34].

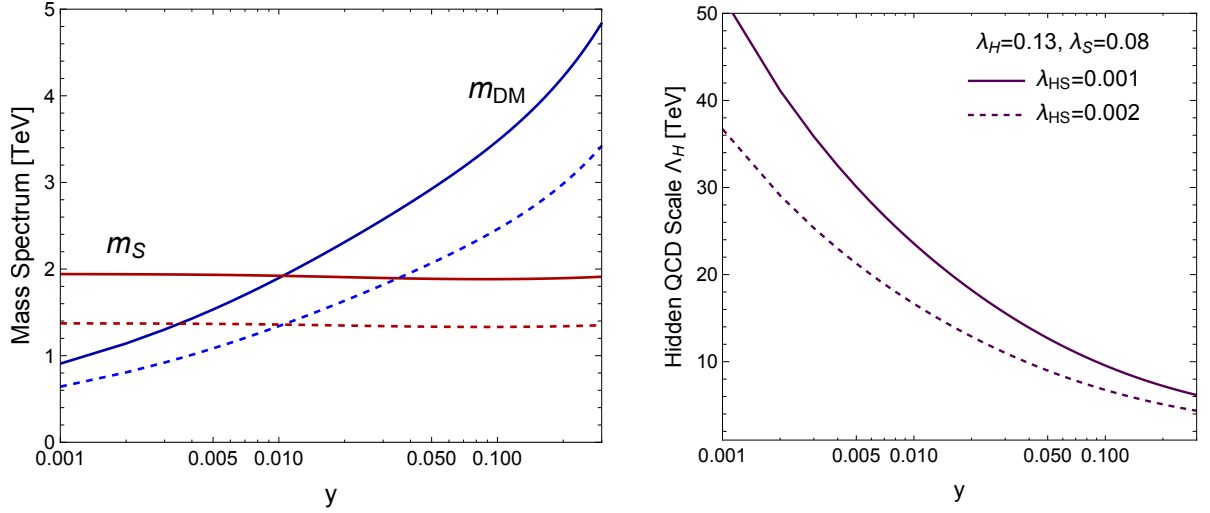


FIG. 1: The DM mass  $m_{DM}$  and the mediator mass  $m_S$  (left) and the hidden QCD scale  $\Lambda_H$  (right) versus  $y$  for  $\lambda_H = 0.13$ ,  $\lambda_S = 0.08$  and  $\lambda_{HS} = 0.001$  (solid lines),  $0.002$  (dashed lines).

### C. Chiral Phase Transitions

The phase transition at finite temperature can be studied using one-loop effective potential. Since the EW phase transition occurs much below the critical temperature of the chiral phase transition in the hidden sector, we may assume  $\langle h \rangle = 0$  in investigating the chiral phase transition. Accordingly, the scalar potential to be analyzed is

$$V_{\text{EFF}}(S, \sigma, T) = V_{\text{SM}+S}^{h \rightarrow 0}(S) + V_{\text{NJL}}(S, \sigma) + V_{\text{CW}}(S) + V_{\text{FT}}(S, \sigma, T) + V_{\text{RING}}(S, T), \quad (17)$$

where  $V_{\text{SM}+S}$  and  $V_{\text{NJL}}$  are given, respectively, in (2) and (9),

$$V_{\text{CW}}(S) = -\frac{9}{4} \frac{\lambda_S^2}{32\pi^2} (S^4 - \langle S \rangle^4) + \frac{m_S^4(S)}{64\pi^2} \ln \left[ \frac{m_S^2(S)}{m_S^2(\langle S \rangle)} \right], \quad (18)$$

$$V_{\text{FT}}(S, \sigma, T) = \frac{T^4}{2\pi^2} J_B(m_S^2(S)/T^2) - 6n_c \frac{T^4}{\pi^2} J_F(M^2(S, \sigma)/T^2), \quad (19)$$

$$V_{\text{RING}}(S, T) = -\frac{T}{12\pi} [(M_S^2(S, T))^{3/2} - (m_S^2(S))^{3/2}], \quad (20)$$

and  $m_S^2(S) = 3\lambda_S S^2 + \mathcal{O}(y^2)$  is the field-dependent mass for  $S$  with its thermal mass

$$M_S^2 = m_S^2(S) + \left( \frac{\lambda_S}{4} - \frac{\lambda_{HS}}{6} \right) T^2. \quad (21)$$

The thermal function is

$$J_{B,F}(r^2) = \int_0^\infty dx x^2 \ln \left( 1 \mp e^{-\sqrt{x^2 + r^2}} \right), \quad (22)$$



for which we use the approximate expression

$$J_{B,F}(r^2) = e^{-r^2} \sum_{n=0}^{40} c_n^{B,F} r^{2n}. \quad (23)$$

#### D. Benchmark Points

As discussed in [34], the chiral phase transition in the hidden sector becomes first order for small  $y \lesssim 0.006$ . We require that perturbativity and stability condition (3) of the scalar potential for  $y \lesssim 0.006$  are satisfied up to the Planck scale at the one-loop level <sup>1</sup>. We find that

$$0.13 \lesssim \lambda_H \lesssim 0.14, \quad 0 < \lambda_{HS} < 0.12, \quad 4\lambda_{HS}^2/\lambda_H < \lambda_S \lesssim 0.23 \quad (24)$$

should be satisfied to meet the requirements. The inequality  $0 < \lambda_{HS}$  is our assumption (see (3)), and the interval of  $\lambda_H$  is due to the observed Higgs mass. The upper limit of  $\lambda_S$  comes from perturbativity, while the lower limit comes from the stability condition with finite  $\lambda_H$  and  $\lambda_{HS}$ . Note that there is no lower limit on  $\lambda_{HS}$  and  $y$ . We however consider only the case for  $\lambda_{HS}, y \gtrsim 10^{-4}$ , which implies that  $\Lambda_H < 200$  TeV <sup>2</sup>.

In Fig. 2 we show the area in the  $m_{\text{DM}}\text{-}\Lambda_H$  plane, in which we obtain the VEV of Higgs field  $\langle h \rangle = 246$  GeV, the correct Higgs mass  $m_h = 125.09 \pm 0.24$  GeV [46],  $h$ - $S$  mixing  $\xi_1^{(1)} > 0.99$  [46] and the resonance condition  $m_S \simeq 2m_{\text{DM}}$  (to realize the correct DM relic abundance). Note that the mass of the mediator  $S$  is bounded, because  $\lambda_S$  is bounded as discussed above. Consequently, because of the resonance condition  $m_S \simeq 2m_{\text{DM}}$ , the DM mass is bounded, too. Similarly,  $\Lambda_H$  is bounded, because  $\lambda_{HS}$  is bounded from above (24) and from below due to our parameter choice  $\lambda_{HS} > 10^{-4}$ . The colored points A, B, C and D in Fig. 2 are our benchmark points.

The chosen four benchmark points are named Case A, B, C and D: the set of the input parameter values  $(\lambda_H, \lambda_{HS}, \lambda_S, y)$  along with the output values of  $m_{\text{DM}}$ ,  $\Lambda_H$  and  $y \langle S \rangle / \Lambda_H$  for each benchmark case is given in Table I. Under  $y \lesssim 0.006$  and (24), the Case A and

<sup>1</sup> According to [47] the hierarchy problem can be avoided in this way at least at the one-loop level.

<sup>2</sup> A large  $\Lambda_H$ , which is realized by the small couplings  $y$  and  $\lambda_{HS}$ , does not necessarily mean a heavy  $S$  as shown in Fig. 1. Therefore, even if  $\Lambda_H$  is large, the correction to the Higgs mass coming from the internal  $S$  loop can be small.

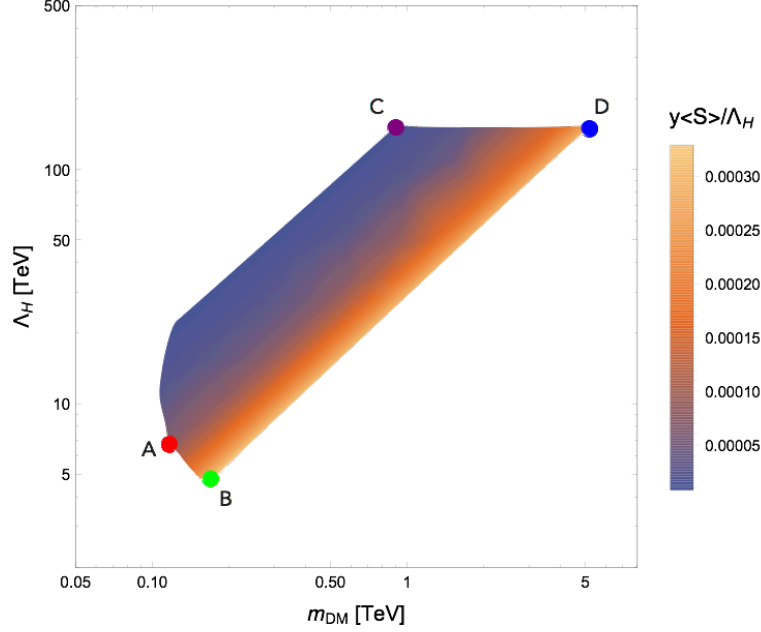


FIG. 2: The hidden QCD scale  $\Lambda_H$  against the DM mass  $m_{DM}$ . In the colored region,  $\langle h \rangle = 246$  GeV,  $m_h = 125.09 \pm 0.24$  GeV,  $\xi_1^{(1)} > 0.99$  ( $h$ - $S$  mixing),  $m_S \simeq 2m_{DM}$ , the perturbativity and stability constraint (24) are satisfied. We assumed the case for  $\lambda_{HS}, y \gtrsim 10^{-4}$ . The color strength indicates the value of  $y \langle S \rangle / \Lambda_H$  which is a measure of how the chiral symmetry is explicitly broken. The colored points are the benchmark points; the Case A (red), B (green), C (purple) and D (blue) which are defined in Table. I.

B locate as close to the EW scale as possible and for C and D in an opposite way<sup>3</sup>. We regard the normalized current quark mass  $y \langle S \rangle / \Lambda_H$  as the characterization for the explicit chiral symmetry breaking. Their values should be compared with that of QCD, i.e.  $m_u / \Lambda_{QCD} \sim 6 \times 10^{-3}$  (in the NJL model).

In Fig. 3 we show the temperature dependence of  $\langle \sigma \rangle / T$  and  $\langle S \rangle / T$  near the critical temperature for each benchmark point. It can be seen that a first-order phase transition appears in all the cases. We also see that  $\sigma$  and  $S$  undergo the phase transition at the same time. Moreover, the phase transition in the Case C appears for a slightly lower temperature compared with D despite of  $\Lambda_H^C > \Lambda_H^D$ . The reason is that the explicit chiral symmetry

<sup>3</sup> There exists the Higgs threshold between the Case A and B, which means the decay channel of the mediator  $S$  to two Higgs particles is forbidden only for the Case A. This might become a benchmark point for the future collider search.

TABLE I: Four benchmark points, the Case A-D, which are defined by the values of  $(\lambda_H, \lambda_{HS}, \lambda_S, y)$ , where  $m_{\text{DM}}$ ,  $\Lambda_H$  and  $y \langle S \rangle / \Lambda_H$  are displayed for each case.

Case	$(\lambda_H, \lambda_{HS}, \lambda_S, y)$	$m_{\text{DM}}$ [TeV]	$\Lambda_H$ [TeV]	$y \langle S \rangle / \Lambda_H$
A	( 0.140, 0.050, 0.054, $8.57 \times 10^{-4}$ )	0.117	6.84	$7.30 \times 10^{-6}$
B	( 0.138, 0.098, 0.230, $3.60 \times 10^{-3}$ )	0.170	4.87	$3.05 \times 10^{-5}$
C	( 0.129, 0.0001, 0.007, $1.07 \times 10^{-4}$ )	0.906	153.1	$8.73 \times 10^{-6}$
D	( 0.130, 0.0001, 0.230, $3.55 \times 10^{-3}$ )	5.20	152.5	$2.90 \times 10^{-5}$

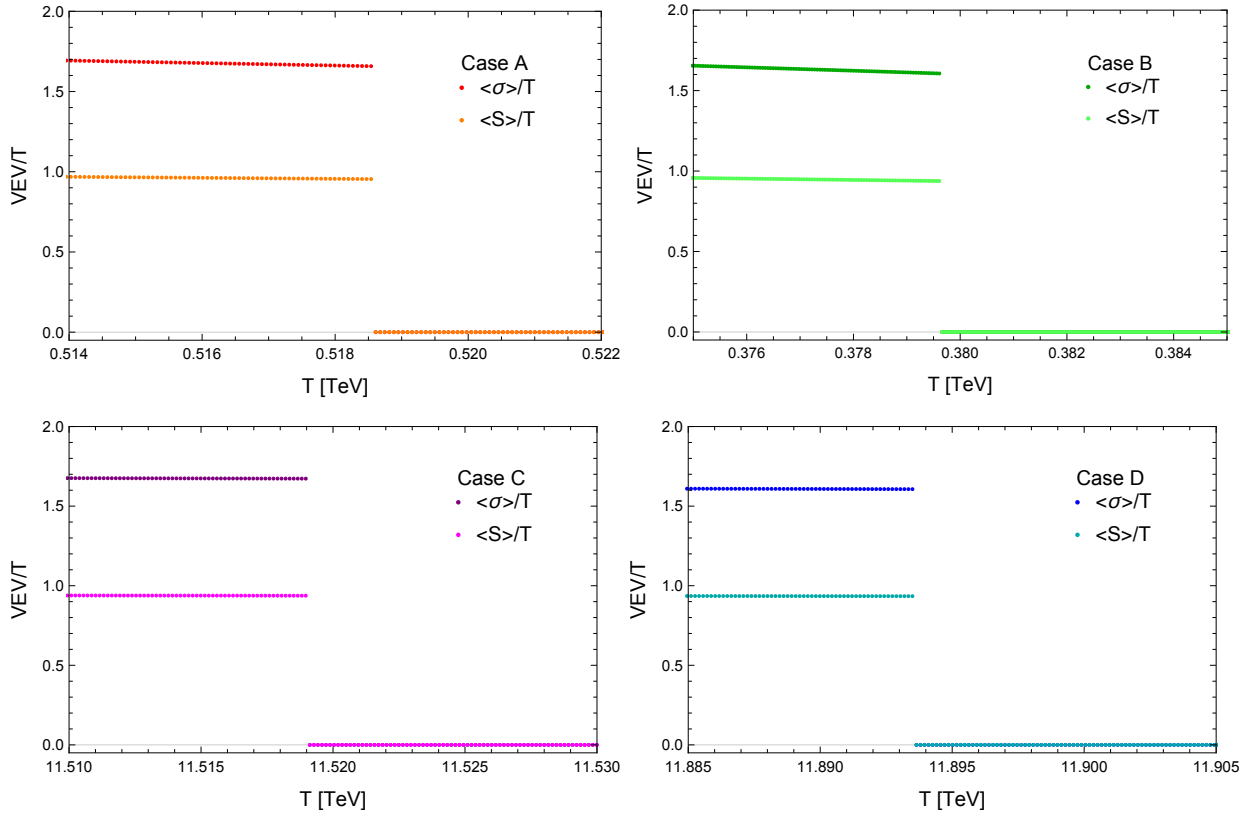


FIG. 3: The temperature dependence of  $\langle \sigma \rangle / T$  (dark-colored) and  $\langle S \rangle / T$  (light-colored) for each benchmark point. The Case A (left-top), B (right-top), C (left-bottom) and D (right-bottom) are defined in Table. I.

breaking, whose strength is expressed by  $y \langle S \rangle / \Lambda_H$ , influences not only the mass of DM but also the critical temperature. Since the chiral phase transition in the hidden sector occurs in the two-dimensional space  $(S, \sigma)$ , we need to deal with a quantum tunneling in the two-dimensional space to calculate the GW spectrum.

### III. BUBBLES FROM HIDDEN QCD TUNNELING

The cosmological tunneling has been studied in [48–50]. The probability of the bubble nucleation per unit volume per unit time is given by

$$\Gamma = A(t) \exp[-S_E(t)], \quad (25)$$

where  $S_E$  is the Euclidean action. At high temperature the Euclidean action can be replaced by  $S_E = S_3/T$  because of the periodicity of  $S_E$  in the Euclidean time, where  $S_3$  is the corresponding three dimensional Euclidean action [50]. The bubbles can percolate when the probability of the bubble nucleation per unit volume and time is of order one. Since the prefactor  $A$  in (25) is  $A(T) \propto T^4$  [50], we can translate this condition as

$$\left. \frac{\Gamma}{H^4} \right|_{t=t_t} \simeq 1 \quad \Leftrightarrow \quad \frac{S_3(T_t)}{T_t} = 4 \ln \left( \frac{T_t}{H_t} \right), \quad (26)$$

where  $H_t$  is the Hubble parameter at the transition temperature  $T_t$ .

The bubble dynamics can be characterized by two parameters, namely  $\alpha$  and  $\beta$  at  $T_t$  [18]:  $\alpha$  expresses how much the phase transition releases the energy, while  $\beta^{-1}$  expresses how long its phase transition takes. These parameters are essential for computing the GW signal from cosmological phase transition [18]. The parameter  $\alpha$  is defined as

$$\alpha \equiv \left. \frac{\epsilon}{\rho_{\text{rad}}} \right|_{T=T_t}, \quad (27)$$

which is the ratio of the latent heat  $\epsilon$  liberated at the phase transition to the thermal energy density  $\rho_{\text{rad}}(T_t) = (\pi^2/30)g_*(T_t)T_t^4$  in the symmetric phase. The latent heat can be computed from effective potential at finite temperature as

$$\epsilon(T) \equiv -\Delta V_{\text{EFF}}(T) + T \frac{\partial \Delta V_{\text{EFF}}(T)}{\partial T}, \quad (28)$$

where  $\Delta V_{\text{EFF}}(T)$  is the difference of the effective potential between the true and false vacuum.

The parameter  $\beta$  is defined as

$$\beta \equiv - \left. \frac{dS_E}{dt} \right|_{t=t_t} \simeq \left. \frac{1}{\Gamma} \frac{d\Gamma}{dt} \right|_{t=t_t}. \quad (29)$$

Using  $H_t$ , we can redefine a dimensionless parameter  $\tilde{\beta}$  as

$$\tilde{\beta} \equiv \frac{\beta}{H_t} = T_t \left. \frac{d}{dT} \left( \frac{S_3(T)}{T} \right) \right|_{T=T_t}. \quad (30)$$

In the following subsections we apply above general formula (26) - (30) to compute the parameters  $(T_t, \alpha, \tilde{\beta})$  for our concrete problem, and we estimate the corresponding GW signal.

### A. Bubble Nucleation and Tunneling Parameters

In order to discuss the bubble nucleation which stems from the first-order chiral phase transition, we need to calculate  $S_3$ . For this purpose we use the effective Lagrangian for the mean field  $\sigma$ . However, the mean field  $\sigma$  can not describe tunneling at a tree-level, because its kinetic term is absent at the tree-level. Hence we compute its kinetic term from the two point function  $\Gamma_{\sigma\sigma}$  at the one-loop level which are given in (12). First we discuss the zero temperature case and define the field renormalization constant  $Z_\sigma$  for the  $\sigma$  field as

$$\Gamma_{\sigma\sigma}(p^2) = \Gamma_{\sigma\sigma}(0) + Z_\sigma^{-1}(S, \sigma)p^2 + \mathcal{O}(p^4),$$

where

$$Z_\sigma^{-1}(S, \sigma) = - \left(1 - \frac{G_D}{4G^2}\sigma\right)^2 3n_c \frac{d}{dp^2} I_{\varphi^2}(p^2, M; \Lambda_H) \Big|_{p^2=0}.$$

Thus the effective Lagrangian for the  $\sigma$  field at the zero temperature is

$$\mathcal{L}_\sigma = \frac{Z_\sigma^{-1}(S, \sigma)}{2} \partial_\mu \sigma \partial^\mu \sigma - V_{\text{eff}}(S, \sigma), \quad (31)$$

where  $V_{\text{eff}}(S, \sigma) = V_{\text{SM}+S}^{h \rightarrow 0}(S) + V_{\text{NJL}}(S, \sigma)$  ( $V_{\text{NJL}}(S, \sigma)$  is given in (9)). Note that the field renormalization constant  $Z_\sigma^{-1}$  at the symmetric phase ( $S = \sigma = 0$ ) diverges (see Appendix A). This is expected, because the composite state  $\sigma$  disappears in the symmetric phase.

As mentioned in the previous section, the hidden QCD tunneling should occur in the two-dimensional field space and could be described by the three dimensional Euclidean action

$$S_3(T) = \int d^3x \left[ \frac{Z_\sigma^{-1}(S, \sigma, T)}{2} (\partial_i \sigma)^2 + \frac{1}{2} (\partial_i S)^2 + V_{\text{EFF}}(S, \sigma, T) \right]. \quad (32)$$

The field renormalization constant at finite temperature is computed in Appendix A and found to be

$$\begin{aligned} & Z_\sigma^{-1}(S, \sigma, T) \\ &= \frac{3n_c}{8\pi^2} \left(1 - \frac{G_D}{4G^2}\sigma\right)^2 \left[ \ln \left(1 + \frac{\Lambda_H^2}{M^2}\right) + \frac{\Lambda_H^2 M^2}{(\Lambda_H^2 + M^2)^2} - 32\pi^2 (A_F(u^2) - B_F(u^2)) \right], \end{aligned} \quad (33)$$

where  $u = M/T$ , and  $M$ ,  $A_F(u^2)$  and  $B_F(u^2)$  are given in Eqs. (7), (A5) and (A6), respectively. In Fig. 4 we show the field dependency of the field renormalization constant  $Z_\sigma(S, \sigma, T)$  for  $S = 0$  and  $T/\Lambda_H = 0, 0.01, 0.02$  and  $0.03$ , which corresponds the black, red, blue and purple line, respectively. As shown in Fig. 4, the field renormalization constant

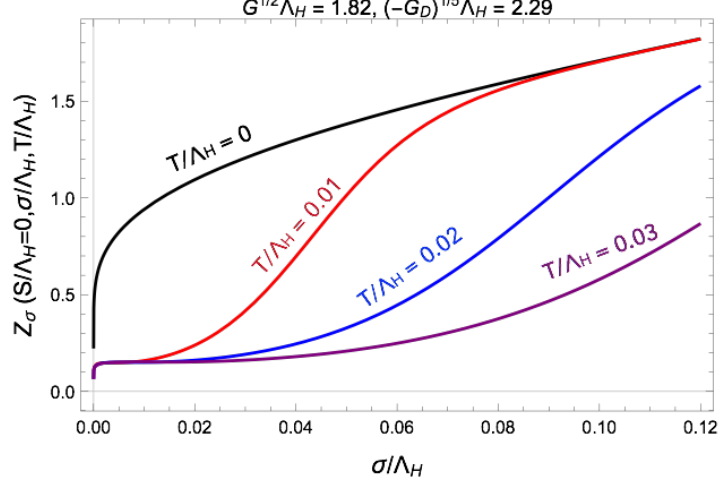


FIG. 4: The  $\sigma$  field dependence of the field renormalization constant  $Z_\sigma(S=0, \sigma, T)$  for  $T/\Lambda_H = 0$  (black), 0.01 (red), 0.02 (blue) and 0.03 (purple).

$Z_\sigma(S, \sigma, T)$  vanishes in the symmetric phase. The  $O(3)$  symmetric bounce solution can be obtained by solving the equations of motion

$$\frac{d^2\sigma}{dr^2} + \frac{2}{r} \frac{d\sigma}{dr} + \frac{1}{2} \frac{\partial \ln Z_\sigma(S, \sigma, T)}{\partial \sigma} \left( \frac{d\sigma}{dr} \right)^2 = Z_\sigma(S, \sigma, T) \frac{\partial V_{\text{EFF}}(S, \sigma, T)}{\partial \sigma}, \quad (34)$$

$$\frac{d^2S}{dr^2} + \frac{2}{r} \frac{dS}{dr} - \frac{1}{2} \frac{\partial Z_\sigma^{-1}(S, \sigma, T)}{\partial S} \left( \frac{d\sigma}{dr} \right)^2 = \frac{\partial V_{\text{EFF}}(S, \sigma, T)}{\partial S}, \quad (35)$$

where  $r = (x_1^2 + x_2^2 + x_3^2)^{1/2}$ . The boundary conditions are

$$\left. \frac{d\sigma}{dr} \right|_{r=0} = 0, \quad \left. \frac{dS}{dr} \right|_{r=0} = 0, \quad \lim_{r \rightarrow \infty} \sigma(r) = 0, \quad \lim_{r \rightarrow \infty} S(r) = 0, \quad (36)$$

where the coordinate of the symmetric minimum (false vacuum) of the potential is chosen at the origin of the  $\sigma$ - $S$  space. Note that the field renormalization constant  $Z_\sigma(S, \sigma, T)$  does not depend explicitly on  $r$  but depends on the fields.

## B. Computation of Multi-dimensional Bounce Solution

In the one-dimensional case we can obtain a bounce solution by using the so-called overshooting/undershooting method [17]. However, this is a cumbersome method in the multi-dimensional case, because two initial conditions have to be simultaneously fine tuned. Instead, we here employ an approach similar to the path deformation method [51].

The bounce solution is unique. That is,  $\sigma(r)$  and  $S(r)$ , which satisfy the differential equations (34) and (35) with the boundary conditions (36), are a unique function of  $r$ . If we assume that  $\sigma(r)$  is an invertible function for  $r \in [0, \infty)$ , then there exists a unique inverse of  $\sigma$ , which we denote by  $\sigma^{-1}$ . That is,  $\sigma^{-1} \circ \sigma$  is the identity function, or  $r = \sigma^{-1}(\sigma(r))$ . Because of this assumption,  $S$  can be regarded as a function of  $\sigma$ , i.e.  $S(\sigma)$ <sup>4</sup>. Therefore, (34) and (35) can be written as, respectively,

$$\frac{d^2\sigma}{dr^2} + \frac{2}{r} \frac{d\sigma}{dr} + \frac{1}{2} \frac{\partial \ln Z_\sigma(S(\sigma), \sigma, T)}{\partial \sigma} \left( \frac{d\sigma}{dr} \right)^2 = F_\sigma(S(\sigma), \sigma), \quad (37)$$

$$\frac{d^2 S}{d\sigma^2} \left( \frac{d\sigma}{dr} \right)^2 + \left( \frac{dS}{d\sigma} \right) \left( \frac{d^2\sigma}{dr^2} + \frac{2}{r} \frac{d\sigma}{dr} \right) - \frac{1}{2} \frac{\partial Z_\sigma^{-1}(S(\sigma), \sigma, T)}{\partial S} \left( \frac{d\sigma}{dr} \right)^2 = F_S(S(\sigma), \sigma), \quad (38)$$

where  $F_\sigma(S(\sigma), \sigma)$  and  $F_S(S(\sigma), \sigma)$  are the rhs of (34) and (35), respectively, and we have suppressed the  $T$  dependence of  $F_\sigma(S(\sigma), \sigma)$  and  $F_S(S(\sigma), \sigma)$ . The point is that if  $S(\sigma)$  is given, then (37) is a one-dimensional differential equation and hence can be solved by applying the overshooting/undershooting method. If  $S(\sigma)$  is the true solution of the problem, it should satisfy (38) with  $\sigma(r)$  obtained from (37) as well, which means that

$$N(r) = 0 \quad (39)$$

is also satisfied, where

$$\begin{aligned} N(r) = & \frac{d^2 S}{d\sigma^2}(r) \left( \frac{d\sigma}{dr}(r) \right)^2 + \frac{dS}{d\sigma}(r) F_\sigma(S, \sigma)(r) - F_S(S, \sigma)(r) \\ & - \frac{1}{2} \left( \frac{d\sigma}{dr}(r) \right)^2 \left( \frac{\partial Z_\sigma^{-1}(S, \sigma, T)}{\partial S}(r) + \frac{dS}{d\sigma}(r) \frac{\partial \ln Z_\sigma(S, \sigma, T)}{\partial \sigma}(r) \right). \end{aligned} \quad (40)$$

Since the one-dimensional differential equation (37) for a given path  $S(\sigma)$  can be simply solved, our task is to find  $S(\sigma)$  which satisfies (39). We do this in an iterative way. We start with a linear function  $S_0(\sigma)$ , which connects the true and false vacuum:

$$S_0(\sigma) = \frac{S^B - S^S}{\sigma^B - \sigma^S} (\sigma - \sigma^S) + S^S, \quad (41)$$

where  $(S^{B,S}, \sigma^{B,S})$  (with  $S^S = \sigma^S = 0$ ) are the position of the true and false vacuum, respectively. Then we solve (37) with the path  $S(\sigma) = S_0(\sigma)$  and denote the bounce solution by  $\sigma_0(r)$ . Note that  $\sigma_0(0)$  is no longer  $\sigma^B$ , so that the end point of  $S_0(\sigma)$  on the true vacuum side is no longer  $S^B$ , i.e.  $S_0(\sigma_0(0)) \neq S^B$ . Next we compute the rhs of (40) using  $\sigma_0(r)$  and

---

<sup>4</sup> We use the same symbol  $S$  for the function of  $r$  and  $\sigma$ .

$S_0(\sigma_0(r))$  for  $\sigma$  and  $S(\sigma)$ , respectively, and we denote it by  $N_0(r)$ . Since  $S_0(\sigma_0(r))$  is not the true solution of the problem,  $N_0(r)$  does not vanish. Knowing  $N_0(r)$ , we have to define the next step of the iteration:

$$S_1(\sigma) = S_0(\sigma) + \Delta S_0(\sigma). \quad (42)$$

To proceed we assume that not only the true solution  $\sigma(r)$  but also  $\sigma_0(r)$  is an invertible function, so that  $N_0(r)$  can be written as a function of  $\sigma$ , i.e.

$$\hat{N}_0(\sigma) \equiv N_0(r = \sigma_0^{-1}(\sigma)). \quad (43)$$

Note that because of the  $\sigma$  and  $S$  dependence of  $Z_\sigma(S, \sigma, T)$  (partly shown in Fig. 4) and also of  $V_{\text{EFF}}(S, \sigma, T)$ ,  $\hat{N}_0(\sigma)$  vanishes at the false vacuum, i.e. at  $\sigma = 0$  ( $S$  also vanishes at  $\sigma = 0$ ). Further, if  $\hat{N}_0(\sigma)$  vanishes at some non-zero values of  $\sigma$ , the deformation  $\Delta S_0(\sigma)$  should also vanish at these values of  $\sigma$ . This brings us to assume that  $\Delta S_0(\sigma)$  is proportional to  $\hat{N}_0(\sigma)$ . Therefore, the path  $S_{i+1}(\sigma)$  in the  $(i+1)$ -th step can be defined as

$$S_{i+1}(\sigma) = S_i(\sigma) + k\hat{N}_i(\sigma), \quad (44)$$

where  $k$  is the step size, and  $\hat{N}_i(\sigma) = N_i(r = \sigma_i^{-1}(\sigma))$ . Note that  $S_{i+1}(\sigma)$  satisfies the boundary condition  $\lim_{\sigma \rightarrow 0} S_{i+1}(\sigma) = 0$ . To obtain  $\sigma_{i+1}(r)$ , the initial value of  $\sigma_{i+1}(0)$  has to be fine tuned in such away that  $d\sigma_{i+1}(r)/dr|_{r=0} = 0$  and  $\lim_{r \rightarrow \infty} \sigma_{i+1}(r) = 0$  are satisfied. If  $d\sigma_{i+1}(r)/dr|_{r=0} = 0$  is satisfied,  $dS_{i+1}(\sigma_{i+1}(r))/dr|_{r=0} = 0$  is automatically satisfied. Since  $\sigma_{i+1}(0)$  is different from  $\sigma_i(0)$ , the end point of  $S_{i+1}(\sigma)$  on the true vacuum side is also moved to  $S_{i+1}(\sigma_{i+1}(0))$ .

Since our assumptions made above cannot be rigorously justified, there is no warranty that the steps converge to the true solution of the problem. In fact, if we choose a wrong sign of  $k$ , steps diverge or do not converge. We have checked our method for a number of examples and found that once we use an appropriate sign and size of  $k$ , the steps can converge, where we approximate the path  $S_i(\sigma)$  (which is obtained numerically) with a fifth-degree polynomial in  $\sigma$  as in [28]. In Fig. 5, we present the numerical solution  $S_{15}(\sigma)$  (black solid) with  $|k\hat{N}_{15}(\sigma)|/S_{15}(\sigma) < 10^{-2}$  obtained from  $S_0(\sigma)$  (black dashed) in the two dimensional field space at  $T = 0.390$  TeV (below the critical temperature  $T = 0.519$  TeV as shown in Fig. 3 (left-top)) for the Case A<sup>5</sup>. The corresponding bounce solution as a function of

---

<sup>5</sup>  $|k\hat{N}_i(\sigma)|/S_i(\sigma) < 10^{-2}$  is not satisfied for  $i < 15$ .



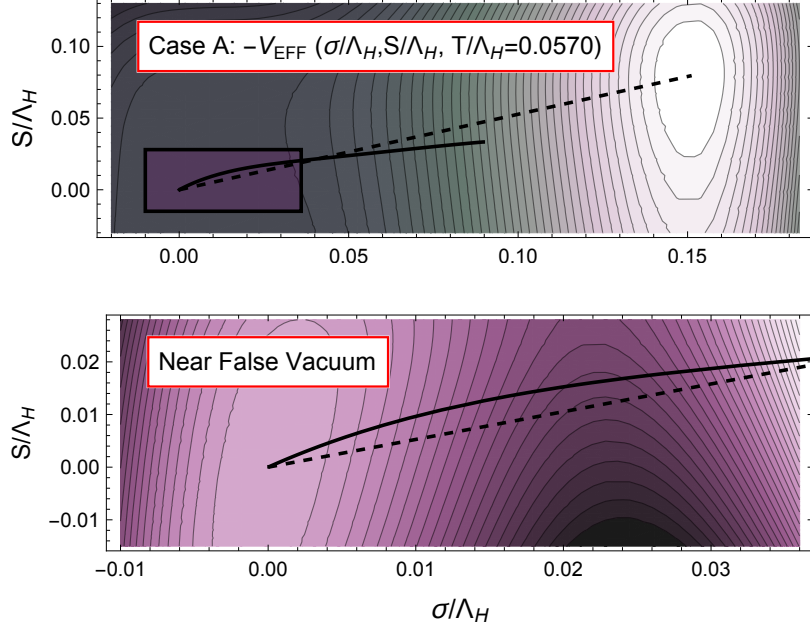


FIG. 5: Top: The contour plot of the effective potential  $V_{\text{EFF}}$  in (17) with  $T/\Lambda_H = 0.0570$  for the Case A defined in Table I. The black-dashed line stands for the initial path  $S_0(\sigma)$  and the black solid line is the path  $S_{15}(\sigma)$  with  $|k\hat{N}_{15}(\sigma)|/S_{15}(\sigma) < 10^{-2}$ . Bottom: The region enclosed by the box near the false vacuum in the top figure is zoomed.

$r$  is shown in Fig. 6. The Euclidean action (32) obtained from the bounce solution is  $S_3(T)/T = 148.2$ , where the difference of  $S_3(T)/T$  between the 14- and 15-th step is less than few percent. Computing  $S_3(T)/T$  for each temperature as above method, we can find the transition temperature  $T_t$  from the condition (26), which is used for the determination of tunneling parameters,  $\alpha$  and  $\tilde{\beta}$  given in Eqs. (27) and (30).

### C. Tunneling Parameters for the Benchmark Points

The GW spectrum produced by a first-order phase transition can be characterized the released energy and its duration time, and it is known that they can be parameterized by the set of the parameters  $(T_t, \alpha, \tilde{\beta})$ . The results for the benchmark points are given in Table II. We see from Table II that  $\alpha$  and  $\tilde{\beta}^{-1}$  for the Case A and C are larger than those for the Case B and D. Recalling the parameter values for the benchmark points (Table I), we can infer that the smaller the explicit chiral symmetry breaking (the smaller  $y$ ) is, the larger  $\alpha$  and  $\tilde{\beta}^{-1}$  are. This suggests that the parameters of the model can be constrained if the GW

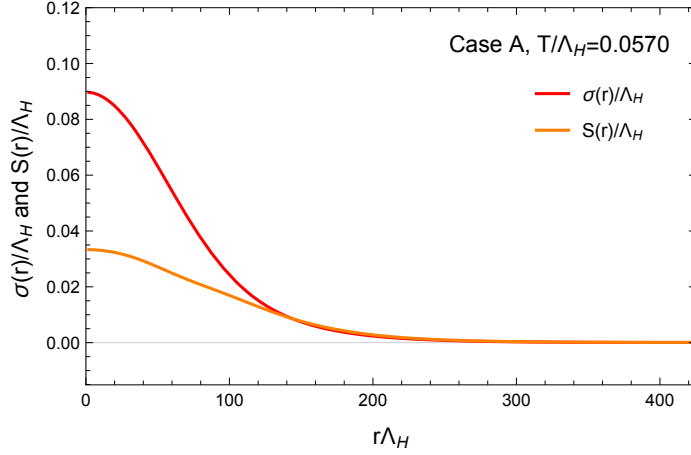


FIG. 6: The bounce solution for the Case A with  $T/\Lambda_H = 0.0570$ . The red line stands for  $\sigma(r)/\Lambda_H$ , and the orange one for  $S(r)/\Lambda_H$ , which correspond to the path (black line) shown in Fig. 5.

TABLE II: The parameters  $(T_t, \alpha, \tilde{\beta})$  for benchmark points defined in Table I. The transition temperature  $T_t$ , the ratio of the latent heat to the thermal energy density  $\alpha$  and the dimensionless inverse duration time  $\tilde{\beta}$  are defined by Eqs. (26), (27) and (30).

Case	$T_t$ [TeV]	$\alpha$	$\tilde{\beta}$
A	0.387	0.288	$8.24 \times 10^2$
B	0.306	0.223	$14.86 \times 10^2$
C	8.731	0.310	$7.15 \times 10^2$
D	9.480	0.232	$13.29 \times 10^2$

is measured with a certain accuracy.

#### IV. SIGNAL FROM THE HIDDEN SECTOR QCD

Finally we come to our main purpose; to check the testability of the GW background produced by the first-order phase transitions in the hidden sector. There coexist three processes contributing to the stochastic GW background spectrum:

$$h^2\Omega_{\text{GW}} = h^2\Omega_\varphi + h^2\Omega_{\text{sw}} + h^2\Omega_{\text{turb}}, \quad (45)$$

where  $h$  is the dimensionless Hubble parameter,  $\Omega_\varphi$  stands for the scalar field contribution from collisions of bubble walls [52–57],  $\Omega_{\text{sw}}$  for the contribution from sound waves in plasma after the bubble collisions [58–61] and  $\Omega_{\text{turb}}$  for the contribution from magnetohydrodynamic (MHD) turbulence in plasma [62–65]. Following [12], each contribution is given for a given set of the parameters  $(T_t, \alpha, \tilde{\beta})$  with the velocity of bubble wall  $v_w$  and the  $\kappa_\varphi$ ,  $\kappa_v$  and  $\kappa_{\text{turb}}$  which are the fraction of vacuum energy, respectively, converted into gradient energy of scalar field, bulk motion of the fluid and MHD turbulence.

- Scalar field contribution  $\Omega_\varphi$ :

$$h^2\Omega_\varphi(f) = 1.67 \times 10^{-5} \tilde{\beta}^{-2} \left( \frac{\kappa_\varphi \alpha}{1 + \alpha} \right)^2 \left( \frac{100}{g_*} \right)^{1/3} \left( \frac{0.11 v_w^3}{0.42 + v_w^2} \right) S_\varphi(f), \quad (46)$$

where the spectral shape of the peak frequency  $f_\varphi$  is

$$S_\varphi(f) = \frac{3.8(f/f_\varphi)^{2.8}}{1 + 2.8(f/f_\varphi)^{3.8}} \quad (47)$$

with the peak frequency

$$f_\varphi = 16.5 \times 10^{-6} \tilde{\beta} \left( \frac{0.62}{1.8 - 0.1 v_w + v_w^2} \right) \left( \frac{T_t}{100 \text{ GeV}} \right) \left( \frac{g_*}{100} \right)^{1/6} \text{ Hz}. \quad (48)$$

- Sound wave contribution  $\Omega_{\text{sw}}$ :

$$h^2\Omega_{\text{sw}}(f) = 2.65 \times 10^{-6} \tilde{\beta}^{-1} \left( \frac{\kappa_v \alpha}{1 + \alpha} \right)^2 \left( \frac{100}{g_*} \right)^{1/3} v_w S_{\text{sw}}(f), \quad (49)$$

where the spectral shape of the peak frequency  $f_{\text{sw}}$  is

$$S_{\text{sw}}(f) = (f/f_{\text{sw}})^3 \left( \frac{7}{4 + 3(f/f_{\text{sw}})^2} \right)^{7/2} \quad (50)$$

with the peak frequency

$$f_{\text{sw}} = 1.9 \times 10^{-5} v_w^{-1} \tilde{\beta} \left( \frac{T_t}{100 \text{ GeV}} \right) \left( \frac{g_*}{100} \right)^{1/6} \text{ Hz}. \quad (51)$$

- MHD turbulence contribution  $\Omega_{\text{turb}}$ :

$$h^2\Omega_{\text{turb}}(f) = 3.35 \times 10^{-4} \tilde{\beta}^{-1} \left( \frac{\kappa_{\text{turb}} \alpha}{1 + \alpha} \right)^{\frac{3}{2}} \left( \frac{100}{g_*} \right)^{1/3} v_w S_{\text{turb}}(f), \quad (52)$$

where the spectral shape of the peak frequency  $f_{\text{turb}}$  is

$$S_{\text{turb}}(f) = \frac{(f/f_{\text{turb}})^3}{[1 + (f/f_{\text{turb}})]^{\frac{11}{3}} (1 + 8\pi f/h_t)} \quad (53)$$

with the peak frequency

$$f_{\text{turb}} = 2.7 \times 10^{-5} v_w^{-1} \tilde{\beta} \left( \frac{T_t}{100 \text{ GeV}} \right) \left( \frac{g_*}{100} \right)^{1/6} \text{ Hz}, \quad (54)$$

and

$$h_t = 16.5 \times 10^{-6} \left( \frac{T_t}{100 \text{ GeV}} \right) \left( \frac{g_*}{100} \right)^{1/6} \text{ Hz}, \quad (55)$$

which is the value (redshifted to today) of the inverse Hubble time at the GW production.

Bubbles produced by quantum tunneling grow with velocity  $v_w$ . It is even possible for  $v_w$  to approach continuously to the speed of light (runaway configuration) [66, 67]. In a no-runaway case, the bubble wall velocity  $v_w$  terminates at a certain velocity  $< 1$ . The criterion for runaway bubbles is the value of  $\alpha$  compared with  $\alpha_\infty$  (the minimum value of  $\alpha$  for runaway bubbles):

- $\alpha_\infty > \alpha$ : No-runaway Bubbles ( $h^2\Omega_{\text{GW}} \simeq h^2\Omega_{\text{sw}} + h^2\Omega_{\text{turb}}$ )
- $\alpha_\infty < \alpha$ : Runaway Bubbles ( $h^2\Omega_{\text{GW}} \simeq h^2\Omega_\varphi + h^2\Omega_{\text{sw}} + h^2\Omega_{\text{turb}}$ ),

where  $\alpha_\infty$  is given by [12, 68]

$$\alpha_\infty \simeq \frac{30}{24\pi^2} \frac{\sum_a c_a \Delta m_a^2(\varphi)}{g_* T_t^2}. \quad (56)$$

Here  $c_a$  is the degree of freedom of the particle  $a$  (which should be multiplied with 1/2 in the fermionic case in addition), and  $\Delta m_a^2(\varphi)$  is the difference of its field-dependent squared masses in two phases. For our model with  $g_* = 115.75$  we use

$$\alpha_\infty \simeq 1.09 \times 10^{-3} \left[ n_f \left( \frac{2M(\langle \varphi_i \rangle)}{T_t} \right)^2 + 3\lambda_S \left( \frac{\langle S \rangle}{T_t} \right)^2 \right]. \quad (57)$$

Here we have used the relation  $m_\sigma^2 \simeq (2M)^2$ , where the constituent mass  $M$  is given in Eq. (7). This relation is approximately satisfied, because we have neglected the contribution from the Yukawa coupling  $y$  (which is very small for our benchmark parameters). We have computed  $\alpha_\infty$  for the benchmark points and found

$$\alpha_\infty = \begin{cases} \text{Case A : 0.116} & \text{Case C : 0.125} \\ \text{Case B : 0.092} & \text{Case D : 0.095} \end{cases}. \quad (58)$$

Comparing  $\alpha$  given in Table II with  $\alpha_\infty$  for each benchmark point we see that the bubbles for all cases run away. With  $\alpha_\infty$  given above we can then compute the fraction  $\kappa$  of the latent heat converted to the relevant contribution to the GW spectrum [12]:

$$\kappa_\varphi \equiv 1 - \frac{\alpha_\infty}{\alpha}, \quad \kappa_v \equiv \frac{\alpha_\infty}{\alpha} \kappa_\infty, \quad \kappa_{\text{turb}} = \epsilon \kappa_v, \quad \kappa_\infty \equiv \frac{\alpha_\infty}{0.73 + 0.083\sqrt{\alpha_\infty} + \alpha_\infty}, \quad (59)$$

where for all the benchmark cases (being all run away) we have assumed that the wall velocity  $v_w$  is close to the speed of light, and  $\epsilon = 0.05$  [12] for the MHD turbulence. With Eqs. (46) - (55), (58) and (59) we are now in position to compute the GW signal for the benchmark cases <sup>6</sup>.

In Fig. 7 we present our results. For each benchmark Case (A-D) we show the GW spectrum with  $v_w = 1$ , where the total GW signal, the sound wave, scalar and MHD turbulence contributions are denoted by the solid, dashed, dotted and dot-dashed lines, respectively. The colored regions show observable regions of different configurations of LISA [12, 13] and DECIGO [14–16]. The label of “LISA-N2A5M5L6” corresponds to the configuration of LISA provided in Table 1 in [12], while the labels “B-DECIGO”, “FP-DECIGO” and “Correlation” are DECIGO designs [14–16]. As we can see from Fig. 7 the sound wave contribution is dominant for all the cases, while the MHD turbulence contribution is negligibly small, so that the peak frequency the GW spectrum is basically that of the sound wave contribution. The contribution MHD turbulence is small because  $\epsilon$  (fraction of turbulent bulk motion) is set to 0.05 [12]. The scalar contribution becomes non-negligible at higher frequencies and consequently changes the slope for this region of frequency. But since it depends on  $\tilde{\beta}^{-2}$  (see Eq. (46)), the sound wave contribution being proportional to  $\tilde{\beta}^{-1}$  is larger for smaller  $\tilde{\beta}$ . The peak frequencies of the Case A and B are  $\sim 0.1$  Hz, while those of C and D are few Hz. The main reason for this difference is the different transition temperature  $T_t$  (see Table II), which once again results from the difference of  $\lambda_{HS}$  (see Table I). Consequently, the GW signal is difficult to be observed at LISA [12, 13]. The peak values of the GW spectrum are  $10^{-12}$  for A and C, while those for B and D are  $10^{-13}$ . Therefore, DECIGO sensitivities [14–16] may be sufficient to observe the signal. Finally we summarize the results for Case A-D in Fig. 8 with the DM mass  $m_{\text{DM}}$  and the hidden QCD scale  $\Lambda_{\text{H}}$ . If Case A and B, and

---

<sup>6</sup> The resent papar [69] is certainly relevant to us. But the paper has appeared after we have completed our calculations.

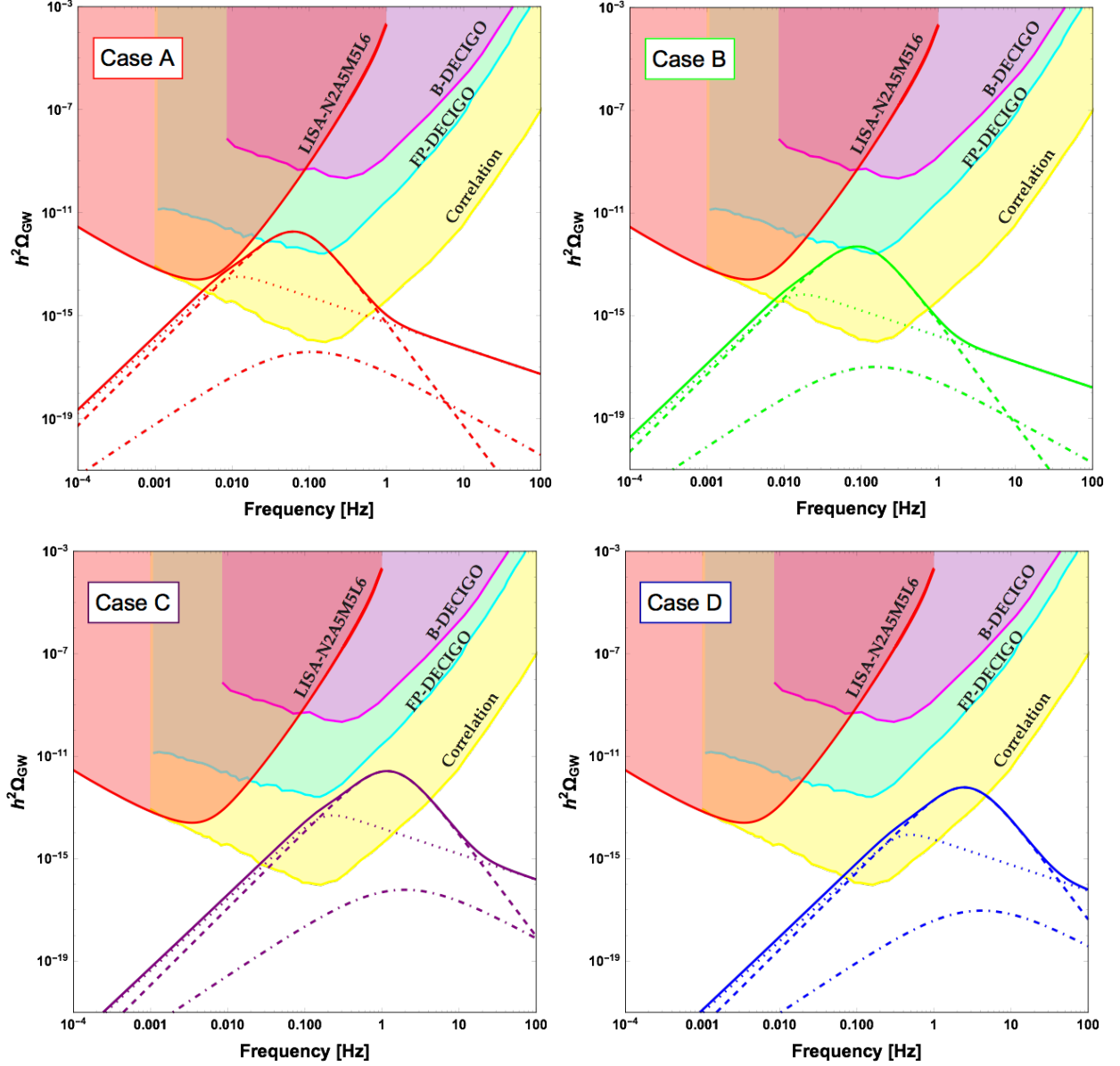


FIG. 7: The GW spectrum with  $v_w = 1$  for the Case A (left-top), B (right-top), C (left-bottom) and D (right-bottom). The total GW spectrum (solid lines) is the sum of the sound wave (dashed lines), scalar (dotted lines) and MHD turbulence (dot-dashed lines) contribution. The colored regions are observable regions of LISA (“LISA-N2A5M5L6”[12]) and DECIGO (“B-DECIGO”, “FP-DECIGO” and “Correlation”[14–16]).

also C and D could be experimentally distinguished, we could obtain the information about the magnitude of the explicit chiral symmetry breaking in the hidden sector.

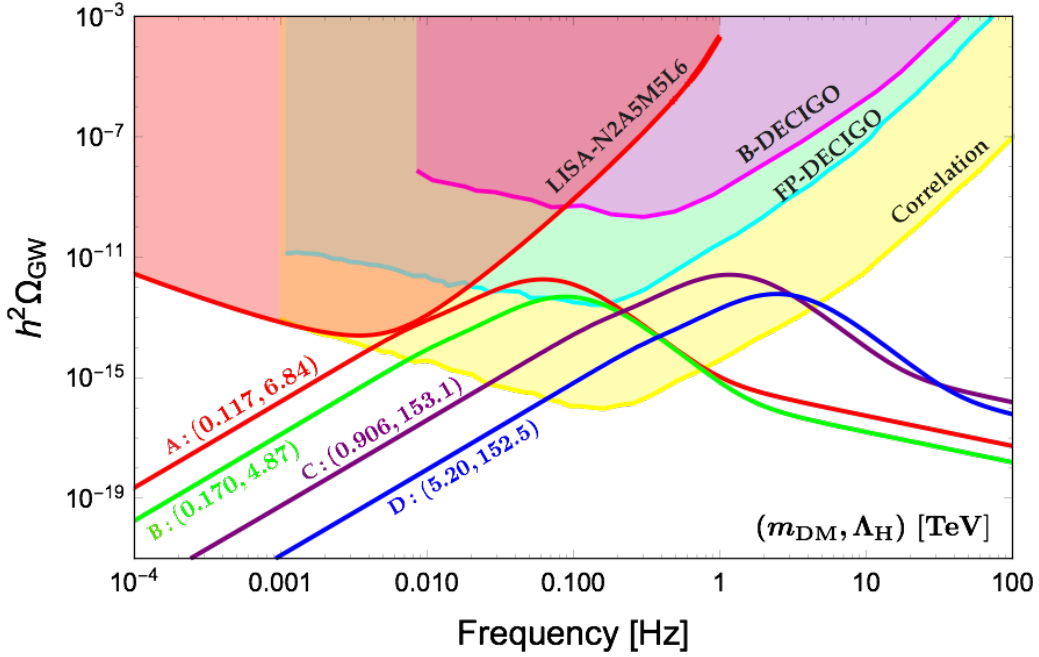


FIG. 8: The GW spectrum with  $v_w = 1$  for the Case A (red), B (green), C (purple) and D (blue). The numbers in the parenthesis are  $m_{\text{DM}}$  and  $\Lambda_{\text{H}}$  in the unit of TeV (Table I). The colored regions are observable regions of LISA (“LISA-N2A5M5L6” [12]) and DECIGO (“B-DECIGO”, “FP-DECIGO” and “Correlation” [14–16]).

## V. SUMMARY AND CONCLUSION

Mass can be created by non-perturbative effects in non-abelian gauge theories “from nothing”. By from nothing we mean that the theory has no dimensional parameter and hence is scale invariant at the classical level. Scale invariance is broken explicitly by scale anomaly and at the same time dynamically by the non-perturbative effects. Dynamical breaking of scale invariance can be used to explain the origin of the Higgs mass as well as of the DM mass [33–39, 70–73].

Needless to say that dynamical breaking of scale invariance is associated with a phase transition at finite temperature [33, 45, 71]. If the phase transition is of first order and strong enough in the early Universe, it can produce GW which might be observed today as a GW background [8].

In this paper we have expanded our analysis of a particular scale invariant extension of the SM to include the aspect of the GW background predicted by the model. The model

contains a strongly interacting hidden sector, described by a non-abelian gauge theory, in which a mass scale in the TeV region is generated through the chiral symmetry breaking in the hidden sector. The corresponding (pseudo) NG bosons are a realistic candidate for DM, where their mass is finite because the chiral symmetry is also explicitly broken by a Yukawa coupling between the hidden sector fermions and a SM singlet real scalar field  $S$ . The scalar field  $S$  plays the role of a mediator that transfers the robust energy scale from the hidden sector to the SM sector via a Higgs portal coupling.

As in [33, 34] we have used the NJL method to effectively treat the  $D\chi$ SB. Integrating out the hidden sector fermions in the NJL model yields an effective potential for the chiral condensate at zero and finite temperature. In the mean field approximation we can identify the chiral condensate with  $\sigma$  and the NG bosons with  $\phi_a$  (which are DM). We have restricted ourselves to  $n_c = n_f = 3$  for the hidden sector QCD, because we can simply scale-up the parameters of the NJL model for the real QCD, such that the hidden sector NJL model has the same number of the independent parameters as that of the hidden sector QCD.

As it is known, the nature of the chiral phase transition changes depending on the strength of the explicit chiral symmetry breaking. For the hidden sector QCD it means, on one hand, that the Yukawa coupling constant  $y$  should be sufficiently small to obtain a strong first-order chiral phase transition. On the other hand, a small  $y$  implies two-stage phase transitions; the chiral phase transition at  $T \gtrsim \mathcal{O}(1)$  TeV and the EW phase transition at  $T \sim \mathcal{O}(100)$  GeV. That is, two phase transitions can be clearly distinguished.

Using the technique in the literature (see [12] and the references therein) within the framework of the NJL model in the mean field approximation, we have analyzed the GW background produced by the chiral phase transition in the hidden sector of the model. In particular, depending on the value of  $y$  and of the Higgs portal coupling  $\lambda_{HS}$ , we have chosen four benchmark points in the parameter space. These points are representative points characterized by the magnitude of the explicit chiral symmetry breaking and the hidden sector scale  $\Lambda_H$ . We have found for these points that the peaks of the GW signal appear at frequencies  $\mathcal{O}(0.01 - 1)$  Hz. Unfortunately, these frequencies are slightly too high, so that it will be difficult for them to be observed at LISA [12, 13]. But their strength seems to be sufficiently large for observations at DECIGO [14–16] which will cover a higher frequency region. We emphasize that observation of a GW background signal at frequencies  $0.1 \sim \text{few Hz}$  with  $h^2\Omega_{\text{GW}} \gtrsim 10^{-13}$  may be a strong indication for strongly interacting hidden



sector models.

Finally we should admit that our results have been obtained by using the NJL model, which is supposed to serve as an effective theory of the hidden sector QCD. A fair question is about the systematic uncertainties present in this approach. At the moment we can say only that the NJL model for the real hadrons can reproduce their basic quantities with an uncertainty of  $\mathcal{O}(10 - 20)\%$  [44]. Therefore, to make more precise predictions it is certainly inevitable to use a more reliable method such as lattice gauge theory.

### Acknowledgments

We thank Thomas Konstandin for useful discussions. The work of M. A. is supported in part by the Japan Society for the Promotion of Sciences Grant-in-Aid for Scientific Research (Grant No. 16H00864 and No. 17K05412). J. K. is partially supported by the Grant-in-Aid for Scientific Research (C) from the Japan Society for Promotion of Science (Grant No.16K05315).

### Appendix A: Thermal Function for Field Renormalization Constant

The field renormalization can be computed as

$$Z_\sigma^{-1}(S, \sigma) = - \left( 1 - \frac{G_D}{4G^2} \sigma \right)^2 3n_c \frac{d}{dp^2} I_{\varphi^2}(p^2, M; \Lambda_H) \Big|_{p^2=0},$$

where the loop function  $I_{\varphi^2}(p^2, M)$  is given in Eq. (13) and its derivative can be written as

$$\begin{aligned} & \frac{d}{dp^2} I_{\varphi^2}(p^2, M) \Big|_{p^2=0} \\ &= -4 \int \frac{d^4 k}{i(2\pi)^4} \frac{1}{(k^2 - M^2)^2} + 4 \int \frac{d^4 k}{i(2\pi)^4} \frac{2M^2}{(k^2 - M^2)^3} \equiv -4I_A(M) + 4I_B(M), \end{aligned}$$

where we defined two terms as  $I_A$  and  $I_B$ . Using the standard calculation method at finite temperature, they can be computed as

$$I_A = \frac{T}{2\pi i} \oint_C \frac{d^3 k}{(2\pi)^3} \frac{1}{(k_0^2 - \omega^2)^2} \frac{1}{2} \beta \tanh \left( \frac{1}{2} \beta k_0 \right) = A_F^0(M; \Lambda_H) + A_F(u^2), \quad (\text{A1})$$

$$I_B = \frac{T}{2\pi i} \oint_C \frac{d^3 k}{(2\pi)^3} \frac{2M^2}{(k_0^2 - \omega^2)^3} \frac{1}{2} \beta \tanh \left( \frac{1}{2} \beta k_0 \right) = B_F^0(M; \Lambda_H) + B_F(u^2), \quad (\text{A2})$$

where  $\beta = 1/T$ ,  $k_0 = i\omega_n = i\pi(2n+1)T$ ,  $u = M/T$  and the function  $\frac{1}{2}\beta \tanh(\frac{1}{2}\beta k_0)$  has pole at  $k_0$ . The zero temperature components with four dimensional cut-off are

$$A_F^0(M; \Lambda_H) = \int_{\Lambda_H} \frac{d^4 k_E}{(2\pi)^4} \frac{1}{(k_E^2 + M^2)^2} = \frac{1}{(4\pi)^2} \frac{1}{2} \left[ \ln \left( 1 + \frac{\Lambda_H^2}{M^2} \right) - \frac{\Lambda_H^2}{\Lambda_H^2 + M^2} \right], \quad (\text{A3})$$

$$B_F^0(M; \Lambda_H) = - \int_{\Lambda_H} \frac{d^4 k_E}{(2\pi)^4} \frac{2M^2}{(k_E^2 + M^2)^3} = - \frac{1}{(4\pi)^2} \frac{\Lambda_H^4}{2(\Lambda_H^2 + M^2)^2}, \quad (\text{A4})$$

and those thermal effect functions can be written as

$$\begin{aligned} A_F(u^2) &= \int_{-i\infty+\epsilon}^{i\infty+\epsilon} \frac{dk_0}{2\pi i} \int \frac{d^3 k}{(2\pi)^3} \frac{2}{(k_0 - \omega)^2 (k_0 + \omega)^2} \frac{1}{e^{\beta k_0} + 1} \\ &= - \frac{1}{4\pi^2} \int_0^\infty dx \frac{x^2}{(\sqrt{x^2 + u^2})^3} \frac{1}{1 + e^{\sqrt{x^2 + u^2}}} \\ &\quad - \frac{1}{8\pi^2} \int_0^\infty dx \frac{x^2}{(\sqrt{x^2 + u^2})^2} \frac{1}{1 + \cosh \sqrt{x^2 + u^2}}, \end{aligned} \quad (\text{A5})$$

$$\begin{aligned} B_F(u^2) &= \int_{-i\infty+\epsilon}^{i\infty+\epsilon} \frac{dk_0}{2\pi i} \int \frac{d^3 k}{(2\pi)^3} \frac{4M^2}{(k_0 - \omega)^3 (k_0 + \omega)^3} \frac{1}{e^{\beta k_0} + 1} \\ &= \frac{2u^2}{\pi^2} \left[ 3 \int_0^\infty dx \frac{x^2}{(\sqrt{x^2 + u^2})^5} \frac{1}{1 + e^{\sqrt{x^2 + u^2}}} \right. \\ &\quad + 3 \int_0^\infty dx \frac{x^2}{(\sqrt{x^2 + u^2})^4} \frac{1}{1 + \cosh \sqrt{x^2 + u^2}} \\ &\quad \left. + \int_0^\infty dx \frac{x^2}{(\sqrt{x^2 + u^2})^3} \frac{1}{1 + \cos \sqrt{x^2 + u^2}} \tanh \left( \frac{1}{2} \sqrt{x^2 + u^2} \right) \right]. \end{aligned} \quad (\text{A6})$$

In this work we fitted each thermal function using the following fitting functions,

$$A_F(u^2) = \frac{1}{8\pi^2} \ln u + e^{-u} \sum_{n=0}^{40} a_n u^n, \quad (\text{A7})$$

$$B_F(u^2) = e^{-u} \sum_{n=0}^{40} b_n u^n. \quad (\text{A8})$$

- 
- [1] ATLAS Collaboration, <https://twiki.cern.ch/twiki/bin/view/AtlasPublic/Winter201713TeV>.
- [2] CMS Collaboration, <https://cms.cern/news/cms-new-results-Moriond-2017>.
- [3] D. S. Akerib *et al.* [LUX Collaboration], Phys. Rev. Lett. **118** (2017) no.2, 021303 [arXiv:1608.07648 [astro-ph.CO]].
- [4] E. Aprile *et al.* [XENON Collaboration], arXiv:1705.06655 [astro-ph.CO].

- [5] B. P. Abbott *et al.* [LIGO Scientific and Virgo Collaborations], Phys. Rev. Lett. **116** (2016) no.6, 061102 [arXiv:1602.03837 [gr-qc]].
- [6] A. A. Starobinsky, JETP Lett. **30** (1979) 682 [Pisma Zh. Eksp. Teor. Fiz. **30** (1979) 719].
- [7] A. Vilenkin and E. P. S. Shellard, “Cosmic Strings and Other Topological Defects,” Cambridge University Press, 2000.
- [8] E. Witten, Phys. Rev. D **30** (1984) 272.
- [9] K. Kajantie, M. Laine, K. Rummukainen and M. E. Shaposhnikov, Nucl. Phys. B **466** (1996) 189 [hep-lat/9510020].
- [10] K. Kajantie, M. Laine, K. Rummukainen and M. E. Shaposhnikov, Phys. Rev. Lett. **77** (1996) 2887 [hep-ph/9605288].
- [11] K. Rummukainen, M. Tsypin, K. Kajantie, M. Laine and M. E. Shaposhnikov, Nucl. Phys. B **532** (1998) 283 [hep-lat/9805013].
- [12] C. Caprini *et al.*, JCAP **1604** (2016) no.04, 001 [arXiv:1512.06239 [astro-ph.CO]].
- [13] H. Audley *et al.*, arXiv:1702.00786 [astro-ph.IM].
- [14] N. Seto, S. Kawamura and T. Nakamura, Phys. Rev. Lett. **87** (2001) 221103 [astro-ph/0108011].
- [15] S. Kawamura *et al.*, Class. Quant. Grav. **23** (2006) S125.
- [16] S. Kawamura *et al.*, Class. Quant. Grav. **28** (2011) 094011.
- [17] R. Apreda, M. Maggiore, A. Nicolis and A. Riotto, Nucl. Phys. B **631** (2002) 342 [gr-qc/0107033].
- [18] C. Grojean and G. Servant, Phys. Rev. D **75** (2007) 043507 doi:10.1103/PhysRevD.75.043507 [hep-ph/0607107].
- [19] J. R. Espinosa, T. Konstandin, J. M. No and M. Quiros, Phys. Rev. D **78** (2008) 123528 [arXiv:0809.3215 [hep-ph]].
- [20] A. Ashoorioon and T. Konstandin, JHEP **0907** (2009) 086 [arXiv:0904.0353 [hep-ph]].
- [21] S. Das, P. J. Fox, A. Kumar and N. Weiner, JHEP **1011** (2010) 108 [arXiv:0910.1262 [hep-ph]].
- [22] P. Schwaller, Phys. Rev. Lett. **115** (2015) no.18, 181101 [arXiv:1504.07263 [hep-ph]].
- [23] M. Kakizaki, S. Kanemura and T. Matsui, Phys. Rev. D **92** (2015) no.11, 115007 doi:10.1103/PhysRevD.92.115007 [arXiv:1509.08394 [hep-ph]].
- [24] R. Jinno and M. Takimoto, Phys. Rev. D **95** (2017) no.1, 015020 doi:10.1103/PhysRevD.95.015020 [arXiv:1604.05035 [hep-ph]].

- [25] K. Hashino, M. Kakizaki, S. Kanemura and T. Matsui, Phys. Rev. D **94** (2016) no.1, 015005 doi:10.1103/PhysRevD.94.015005 [arXiv:1604.02069 [hep-ph]].
- [26] J. Kubo and M. Yamada, JCAP **1612** (2016) no.12, 001 [arXiv:1610.02241 [hep-ph]].
- [27] V. Vaskonen, Phys. Rev. D **95** (2017) no.12, 123515 doi:10.1103/PhysRevD.95.123515 [arXiv:1611.02073 [hep-ph]].
- [28] A. Beniwal, M. Lewicki, J. D. Wells, M. White and A. G. Williams, arXiv:1702.06124 [hep-ph].
- [29] L. Marzola, A. Racioppi and V. Vaskonen, Eur. Phys. J. C **77** (2017) no.7, 484 doi:10.1140/epjc/s10052-017-4996-1 [arXiv:1704.01034 [hep-ph]].
- [30] Y. Aoki, G. Endrodi, Z. Fodor, S. D. Katz and K. K. Szabo, Nature **443** (2006) 675 [hep-lat/0611014].
- [31] P. Petreczky, J. Phys. G **39** (2012) 093002 [arXiv:1203.5320 [hep-lat]].
- [32] T. Bhattacharya *et al.*, Phys. Rev. Lett. **113** (2014) no.8, 082001 [arXiv:1402.5175 [hep-lat]].
- [33] M. Holthausen, J. Kubo, K. S. Lim and M. Lindner, JHEP **1312** (2013) 076 [arXiv:1310.4423 [hep-ph]].
- [34] Y. Ametani, M. Aoki, H. Goto and J. Kubo, Phys. Rev. D **91** (2015) no.11, 115007 [arXiv:1505.00128 [hep-ph]].
- [35] T. Hur, D. W. Jung, P. Ko and J. Y. Lee, Phys. Lett. B **696** (2011) 262 doi:10.1016/j.physletb.2010.12.047 [arXiv:0709.1218 [hep-ph]].
- [36] T. Hur and P. Ko, Phys. Rev. Lett. **106** (2011) 141802 [arXiv:1103.2571 [hep-ph]].
- [37] M. Heikinheimo, A. Racioppi, M. Raidal, C. Spethmann and K. Tuominen, Mod. Phys. Lett. A **29** (2014) 1450077 doi:10.1142/S0217732314500771 [arXiv:1304.7006 [hep-ph]].
- [38] J. Kubo, K. S. Lim and M. Lindner, JHEP **1409** (2014) 016 [arXiv:1405.1052 [hep-ph]].
- [39] H. Hatanaka, D. W. Jung and P. Ko, JHEP **1608** (2016) 094 doi:10.1007/JHEP08(2016)094 [arXiv:1606.02969 [hep-ph]].
- [40] Y. Nambu, Phys. Rev. Lett. **4** (1960) 380.
- [41] Y. Nambu and G. Jona-Lasinio, Phys. Rev. **122** (1961) 345.
- [42] Y. Nambu and G. Jona-Lasinio, Phys. Rev. **124**, 246 (1961).
- [43] T. Kunihiro and T. Hatsuda, Prog. Theor. Phys. **71** (1984) 1332.
- [44] T. Hatsuda and T. Kunihiro, Phys. Rept. **247** (1994) 221 [hep-ph/9401310].
- [45] K. Tsumura, M. Yamada and Y. Yamaguchi, arXiv:1704.00219 [hep-ph].
- [46] C. Patrignani *et al.* [Particle Data Group], Chin. Phys. C **40** (2016) no.10, 100001.

- [47] W. A. Bardeen, FERMILAB-CONF-95-391-T.
- [48] S. R. Coleman, Phys. Rev. D **15** (1977) 2929 Erratum: [Phys. Rev. D **16** (1977) 1248].
- [49] C. G. Callan, Jr. and S. R. Coleman, Phys. Rev. D **16** (1977) 1762.
- [50] A. D. Linde, Nucl. Phys. B **216** (1983) 421 Erratum: [Nucl. Phys. B **223** (1983) 544].
- [51] C. L. Wainwright, Comput. Phys. Commun. **183** (2012) 2006 [arXiv:1109.4189 [hep-ph]].
- [52] A. Kosowsky, M. S. Turner and R. Watkins, Phys. Rev. D **45** (1992) 4514.
- [53] A. Kosowsky, M. S. Turner and R. Watkins, Phys. Rev. Lett. **69** (1992) 2026.
- [54] A. Kosowsky and M. S. Turner, Phys. Rev. D **47** (1993) 4372 [astro-ph/9211004].
- [55] M. Kamionkowski, A. Kosowsky and M. S. Turner, Phys. Rev. D **49** (1994) 2837 [astro-ph/9310044].
- [56] C. Caprini, R. Durrer and G. Servant, Phys. Rev. D **77** (2008) 124015 [arXiv:0711.2593 [astro-ph]].
- [57] S. J. Huber and T. Konstandin, JCAP **0809** (2008) 022 [arXiv:0806.1828 [hep-ph]].
- [58] M. Hindmarsh, S. J. Huber, K. Rummukainen and D. J. Weir, Phys. Rev. Lett. **112** (2014) 041301 [arXiv:1304.2433 [hep-ph]].
- [59] J. T. Giblin, Jr. and J. B. Mertens, JHEP **1312** (2013) 042 [arXiv:1310.2948 [hep-th]].
- [60] J. T. Giblin and J. B. Mertens, Phys. Rev. D **90** (2014) no.2, 023532 [arXiv:1405.4005 [astro-ph.CO]].
- [61] M. Hindmarsh, S. J. Huber, K. Rummukainen and D. J. Weir, Phys. Rev. D **92** (2015) no.12, 123009 [arXiv:1504.03291 [astro-ph.CO]].
- [62] C. Caprini and R. Durrer, Phys. Rev. D **74** (2006) 063521 [astro-ph/0603476].
- [63] T. Kahniashvili, A. Kosowsky, G. Gogoberidze and Y. Maravin, Phys. Rev. D **78** (2008) 043003 [arXiv:0806.0293 [astro-ph]].
- [64] T. Kahniashvili, L. Campanelli, G. Gogoberidze, Y. Maravin and B. Ratra, Phys. Rev. D **78** (2008) 123006 Erratum: [Phys. Rev. D **79** (2009) 109901] [arXiv:0809.1899 [astro-ph]].
- [65] T. Kahniashvili, L. Kisslinger and T. Stevens, Phys. Rev. D **81** (2010) 023004 [arXiv:0905.0643 [astro-ph.CO]].
- [66] D. Bodeker and G. D. Moore, JCAP **0905** (2009) 009 [arXiv:0903.4099 [hep-ph]].
- [67] D. Bodeker and G. D. Moore, arXiv:1703.08215 [hep-ph].
- [68] J. R. Espinosa, T. Konstandin, J. M. No and G. Servant, JCAP **1006** (2010) 028 [arXiv:1004.4187 [hep-ph]].

- [69] R. Jinno, S. Lee, H. Seong and M. Takimoto, arXiv:1708.01253 [hep-ph].
- [70] J. Kubo and M. Yamada, Phys. Rev. D **93** (2016) no.7, 075016  
doi:10.1103/PhysRevD.93.075016 [arXiv:1505.05971 [hep-ph]].
- [71] J. Kubo and M. Yamada, PTEP **2015** (2015) no.9, 093B01 doi:10.1093/ptep/ptv114  
[arXiv:1506.06460 [hep-ph]].
- [72] H. Ishida, S. Matsuzaki, S. Okawa and Y. Omura, Phys. Rev. D **95** (2017) no.7, 075033  
doi:10.1103/PhysRevD.95.075033 [arXiv:1701.00598 [hep-ph]].
- [73] N. Haba and T. Yamada, Phys. Rev. D **95** (2017) no.11, 115016  
doi:10.1103/PhysRevD.95.115016 [arXiv:1701.02146 [hep-ph]].